J Therm Anal Calorim (2011) 104:549–554
DOI 10.1007/s10973-010-1097-x

Thermal and electrochemical study of solid-state reaction of mercury with Pt–20% Rh alloy

Gisele Cristiane Becher Ribas · Gledison Rogério de Souza · Fernando Luis Fertonani

Received: 29 July 2009 / Accepted: 6 October 2010 / Published online: 25 November 2010

Abstract Thermogravimetry (TG), energy dispersive X-ray microanalysis (EDX), scanning electron microscopy (SEM), mapping surface and X-ray diffraction (XRD) have been used to study the reaction of mercury with platinum–rhodium (Pt–Rh) alloy. The results suggest that, when heated, the electrodeposited Hg film reacts with Pt–Rh to form intermetallic compounds each having a different stability, indicated by separate third mass-loss steps. In the first step, between room temperature and 170 °C, only the bulk Hg is removed. From this temperature to about 224 °C, the mass loss can be attributed to decomposition of the intermetallic $PtHg_4$. The third step, from 224 to 305 °C, can be ascribed to thermal decomposition of solid solution composed of intermetallic species $RhHg_2$ and $PtHg_2$. Intermetallic compound such as $PtHg_4$, $PtHg_2$, and $RhHg_2$ was characterized by XRD. These intermetallic compounds were the main products formed on the surface of the samples after partial removal of the bulk mercury via thermal desorption.

Keywords Platinum · Rhodium · Mercury · Thermogravimetry · SEM · XRD

G. C. B. Ribas · G. R. de Souza
São Paulo State University (UNESP), IQ/CAr, Rua Francisco Degni s/n, Araraquara, São Paulo, Brazil
e-mail: gigicri@gmail.com

F. L. Fertonani (✉)
São Paulo State University (UNESP), IBILCE, Rua Cristovão Colombo, São José do Rio Preto, São Paulo 2265, Brazil
e-mail: fertonan@iq.unesp.br

Introduction

In recent works, Pt, Rh, Ir, and their alloys have many technological applications: as a catalyst in the petroleum cracking industry; as a catalyst supported on alumina [1], on SiC; as a catalyst support in exhaust catalysts source [2]; on SiO_2 and TiO_2 in the automotive exhaust gas oxidation NO to NO_2 and SO_2 to SO_3 [3, 4]; as a chemical catalyst material in ammonia oxidation plants [5], and in many other electrical devices [6]; as microelectrodes and ultra-microelectrodes in electrochemistry [7, 8].

The existence of mercury in the atmosphere and troposphere as pollutant promotes the contamination of many different kinds of materials and makes possible a great number of chemical and electrochemical processes. Mercury present on noble metals and their alloys can also invalidate their utilization, for example, as standard mass prototype, electrical contact in electrical and electronic devices due to the new species formed, and oxide formation [6, 9, 10].

Mercury interacts easily with these noble metals and with their alloys [10–15], which can be an advantage or a disadvantage depending on the application of the resulting material. Thus, as Hg can be present in petroleum as a contaminant, some problems appear mainly due to the formation of solid intermetallic compounds, since they can modify the catalytic properties in petroleum cracking process. On the other hand, Pt, Hg, and other metals can be electrodeposited on conductive diamond thin-film surfaces to produce novel catalytic electrodes, sensors, and detectors [6].

Recently, solid-state reactions of mercury with Pt, Rh, and Ir, along with some alloys, namely Pt–Ir (20 mass%), Pt–Rh (10 mass%), and Pt–Ir (30 mass%) were studied using different techniques [11, 16–23]. The results allowed

us to suggest that the electrodeposited mercury film, when heated, reacts with Pt, Pt–Rh (10 mass%), and Pt–Ir (20 mass%) alloys to form products having different stabilities, indicated by more than one mass-loss step. These mass-loss steps were associated to the following factors: bulk Hg removal, monolayer mercury desorption, thermal decomposition of intermetallic compounds, and mercury removal from a solid solution of Pt and Pt–Ir alloy containing mercury.

In the present work, mercury films were electrodeposited on Pt–Rh (20 mass%) alloy foils, and the mercury was removed by thermal desorption, as described previously [11, 16–23], and by anodic striping. At the end of each step of the thermal mercury removal, the sample surface was examined using XRD, scanning electron microscopy (SEM), and energy dispersive X-ray microanalysis (EDX). These techniques allowed to characterize, in details, the nature of the intermetallic phases formed on the surface of these metal–mercury systems.

Experimental

Pt–20% Rh (Heraeus Vectra) foils were used as substrate. The foils were polished with α-Al_2O_3 (particles size <0.3 μm) aqueous suspension and washed in HNO_3:H_2O (50% v/v) using an ultrasonic bath. They were then submitted to the following heat treatments: heating at 1200 °C for 4 h and quenching in oxygen-free water at 0 °C. Each sample was treated with HNO_3:HCl (1:3 v/v) solution for 60 s and finally cleaned with a concentrated HF solution at 50 °C for 24 h. Suprapure acids (Merck) and with high purity (18 MΩ cm) were used. For mercury deposition, an Ecochemie Potenciost-Galvanostat PGSTAT10 and a washing electrochemical cell (10 mL) to allow matrix solution exchange were used. A Pt–20% Rh foil (3 mm × 12.5 mm × 60 μm) was used as working electrode. A large platinum gauze (around 1 cm^2) (Heraeus Vectra) was the counter-electrode and an Ag|AgCl|$KNO_{3(sat)}$, $AgCl_{(sat)}$ the reference electrode. This reference was used to substitute the double junction electrode to avoid Hg_2Cl_2 precipitation at the junction for long time experiments. First, a cyclic voltammogram in the supporting electrolyte solution with $E_{inicial} = E_{final} = 0.8$ V; $E_{\lambda,1} = -0.15$ V; and $E_{\lambda,2} = 1.15$ V at 100 mV s^{-1} was recorded. Afterward, the mercury was deposited from a degassed solution containing mercurosos ions, applying −0.30 V for 300 s. Thermogravimetry (TG) experiments were performed using foils with mercury electrodeposited. TG curves were recorded from 30 to 800 °C, at $\beta = 5$ °C min^{-1}, under a purified N_2 atmosphere flux of about 150 mL min^{-1}, using SDT 2960-Simultaneous DSC-TGA-TA Instruments. An α-alumina crucible with a perforated lid ($\phi = 1$ mm) was used to obtain the TG curve.

For cyclic voltammetric studies, the foils were polished and cleaned as above described. Then, the foils were submitted to electrochemical measurements in 1.00 mol dm^{-3} KNO_3/HNO_3 (pH 1) with different concentrations of mercurosos ions ($C_{Hg(I)}$) solution prepared from a $C_{Hg(I)} = 60.0 \times 10^{-3}$ mol L^{-1} stock solution. The electrodes, electrochemical cell, and equipments were the same above described. Single and consecutive cyclic voltammograms were performed at different scan rate, and the inset in the figures shows the potential program applied.

The sample surfaces before and after they had been heated up to different temperatures were examined using a JEOL JSM-T330A (JEOL, Ltd., Akishima, Japan) microscope with a NORAN EDX (Thermo Electron Corporation, Waltham, MA) coupled system in order to take SEM images and mapping of the elements, and a D-5000 SIEMENS X-ray diffractometer (Siemens D500, Karlsrube, Germany) was implemented to obtain the patterns diffractions.

The data generated from the XRD studies were treated using AFPAR software (Complex des Programme, CNRS, France). This program was utilized to determine the lattice parameters of the possible species formed on the Rh foil surface. This method makes use of the Experimental Interplanar Spacings (d-spacing) and data on an original prototype, such as $RhHg_2$ (values of lattice parameters and the respective reflections), which were put together to obtain the experimental lattice parameters.

Results and discussion

Figure 1 shows the TG and DTG curves for Pt–20% Rh/Hg system. The analysis of the TG curve allow us suggest that the mass-loss occurs in three well-defined steps what is

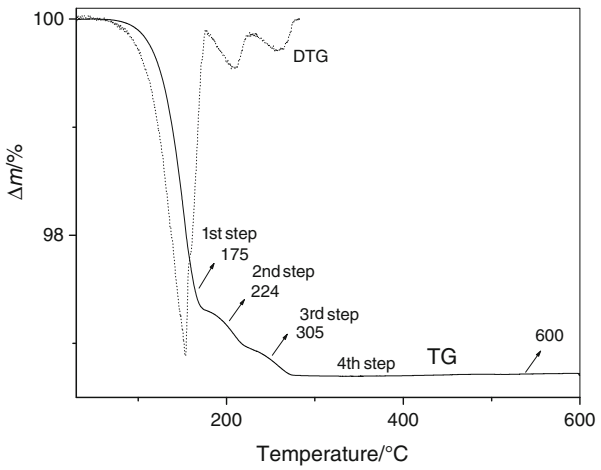

Fig. 1 TG and curves obtained for Pt–20% Rh/Hg from 30 to 700 °C; $\beta = 5$ °C min^{-1}; N_2 flux: 150 cm^3 min^{-1}

supported by the DTG curve. However, observing the final stage of the curve, a region of temperatures between 305 and 600 °C, there is a loss of mass of slow kinetics, corresponding to the fourth and final step of TG curve. The first mass-loss step, from 55 to 175 °C in TG/DTG curves, occurs as a very rapid process and can be attributed to the loss of electrodeposited mercury bulk in agreement with the results already described [11, 15, 18, 21, 22, 24]. The quantity of Hg lost in this step corresponds to 80.8% of the total electrodeposited Hg. Comparing these findings with those for Pt–15% Rh system, a significant increase in the quantity of bulk Hg lost was found for Pt–20% Rh (69%) versus 35% for Pt–15% Rh (values considering the area of foils). This result is coherent with a lower quantity of Hg interacting with the substrate containing 20% of Rh, since it is less reactive. This mercury contents completely "wets" the foil surface because mercury has a lower mercury-substrate contact angle.

Figure 2a shows the SEM image of the of Pt–20% Rh alloy surface after electrodeposition and heating up to a temperature corresponding to the end of the first step in the TG curve. This figure reveals a surface with a film of intermetallic compounds. The film is not uniformly distributed on the surface of the substrate, exposing regions of the substrate, apparently not attacked or subjected to a less aggressive action by the Hg. The results of the mapping of the elements for Pt, Rh, and Hg (Fig. 2b–d) show a large amount of Hg present on the substrate and the homogeneous distribution on the surface, covering the region of grain and grain boundaries.

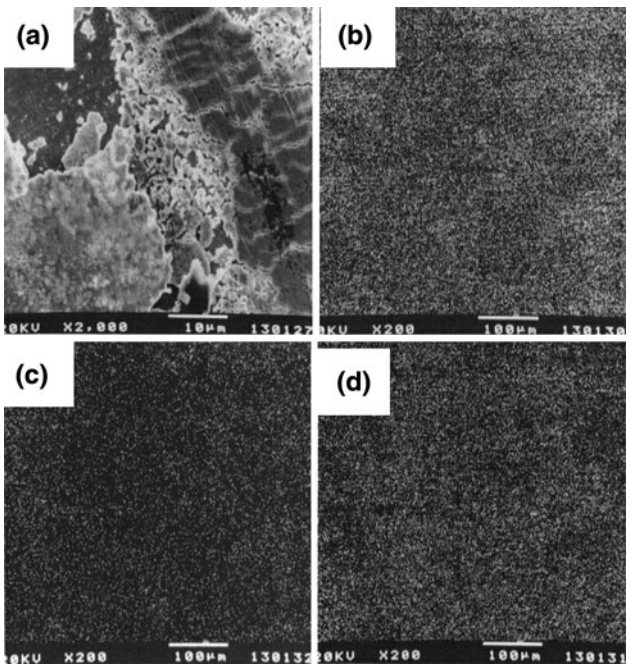

Fig. 2 SEM images and Hg mappings of quenched Pt–20% Rh surface after mercury electrodeposition and heating up to different temperatures: **a** SEM, 175 °C; **b** Pt mapping; **c** Rh mapping; **d** Hg mapping

The EDX microanalysis (Fig. 5a) results revealed a large amount of Hg on the sample surface to the end of the first mass-loss step of TG curve (Fig. 1; T = 275 °C). This amount of Hg is due the presence of an intermetallic film on the substrate as characterized by XRD (Table 1) and in agreement with the results of SEM images (Fig. 2).

The second step of the TG curve, in a temperature range from 175 to 224 °C (Fig. 1), the mass loss was about 11.0% of the total electrodeposited Hg on the Pt–20% Rh foil. This step is related to the second peak of DTG curve, with maximum at 209 °C and is attributed to decomposition of the intermetallic $PtHg_4$, previously determined by X-ray diffractometry (Table 1), according to the reaction:

$$\left[PtHg_{4(s)} + RhHg_{2(s)} + PtHg_{2(s)}\right]_{\text{solid solution}} \rightarrow RhHg_{2(s)} + 2PtHg_{2(s)} + 2Hg_{(v)}.$$

Figure 3 shows the SEM images of the alloy after partial mercury remotion by heating up to temperatures corresponding to the final of the second steps of the TG curve shown in Fig. 1. For temperatures ranging from 175 to 224 °C, the mass loss is 11.0% of the total mercury electrodeposited for the second step. The film of intermetallic compounds does not completely cover the surface, indicating that the film was decomposed. The EDX microanalysis (Fig. 5) results, and mapping of Pt, Rh,

Table 1 XRD experimental data obtained for the quenched Pt–20% Rh foil surface heating up to $T = 175$ °C; $\beta = 5$ °C min^{-1}: N_2 flow rate: 150 mL min^{-1}; Cu $K_\alpha = 1.5405$ Å

2θ	$d_{exp.}$	$d^{a}_{tab.}$	Compound
20.34	4.367	4.37	$PtHg_4/PtRh$
28.84	3.093	3.09	$PtHg_4$
35.50	2.523	2.52	$PtHg_4$
40.27	2.236	–	PtRh
41.20	2.189	2.19	$PtHg_4/RhHg_2$
44.55	2.024	2.04	HgO
46.80	1.940	1.95	$PtHg/PtHg_4/PtRh$
51.00	1.789	1.79	$PtHg_4$
52.04	1.758	1.76	Pt_3O_4
55.53	1.654	1.65	$PtHg_2/PtHg_4$
57.60	1.614	1.61	$RhHg_2$
59.53	1.552	1.55	$PtHg_4$
63.79	1.459	1.46	$PtHg_4$
64.64	2.442	1.44	$PtHg_2/RhHg_2$
67.55	1.385	1.38	$PtHg_4$
68.30	1.373	1.37	$PtHg_2$

[a] Obtained from [24]

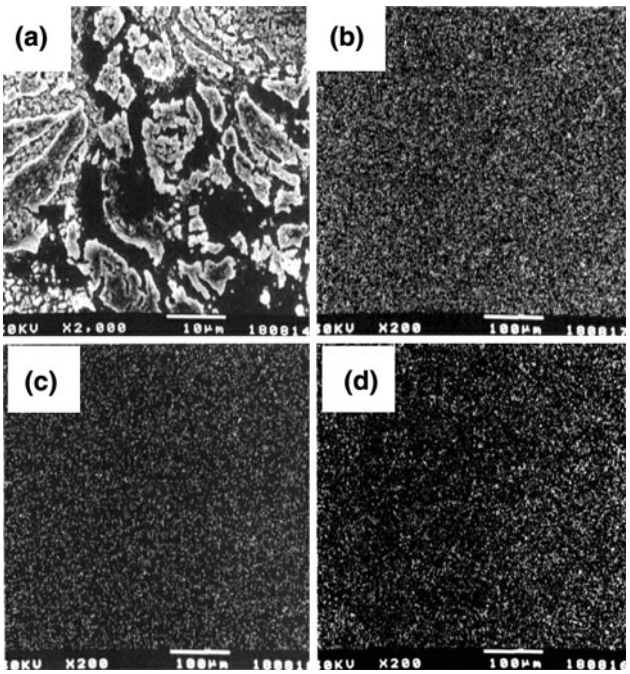

Fig. 3 SEM images and Hg mappings of quenched Pt–20% Rh surface after mercury electrodeposition and heating up to different temperatures: **a** SEM, 224 °C; **b** Pt mapping; **c** Rh mapping; **d** Hg mapping

Table 2 XRD experimental data obtained for the quenched Pt–20% Rh foil surface heating up to $T = 224$ °C; $\beta = 5$ °C min^{-1}: N_2 flow rate: 150 mL min^{-1}; Cu $K_\alpha = 1.5405$ Å

2θ	$d_{exp.}$	$d^{a}_{tab.}$	Compound
19.07	4.631	4.66	$PtHg_2$
21.25	4.208	4.20	PtHg
27.16	3.277	3.29	$PtHg_2$
30.33	2.955	2.96	PtHg
34.95	2.571	2.57	PtO_2
36.11	2.489	2.49	$RhHg_2$
38.84	2.321	2.33	$PtHg_2$
41.15	2.193	2.19	$RhHg_2$
46.63	1.940	1.95	PtHg
49.93	1.823	1.82	$PtHg_2$
68.27	1.372	1.37	$PtHg_2$

[a] Obtained from [24]

and Hg (Fig. 3b–d) shows a decrease in the amount of Hg due to the thermal decomposition of the species $PtHg_4$. The maps shown in Fig. 3b–d, in connection with the results of EDX microanalysis (Fig. 5), indicate an enrichment in Pt and suggest the same for Rh, but at lower intensity, when compared to the previous condition (175 °C). The results of XRD (Table 2) and Hg mapping (Fig. 3d), obtained for

Table 3 XRD experimental data obtained for the quenched Pt–20% Rh foil surface heating up to $T = 305$ °C and $T = 600$ °C; $\beta = 5$ °C min^{-1}: N_2 flow rate: 150 mL min^{-1}; Cu $K_\alpha = 1.5405$ Å

2θ	$d_{exp.}$	$d^{a}_{tab.}$	Compound
$T = 305$ °C			
21.25	4.184	4.20	PtHg
23.70	3.756	–	PtRh
40.27	2.238	–	PtRh
46.77	1.938	1.95	PtHg
51.77	1.766	1.76	Pt_3O_4
58.10	1.588	1.58	PtO_2
61.16	1.515	1.51	HgO
68.27	1.372	1.37	$PtHg_2$
21.25	4.173	4.20	PtRh
$T = 600$ °C			
22.49	3.952	3.95	Pt_3O_4
23.65	3.751	–	PtRh
27.65	3.236	3.22	Pt_3O_4
40.22	2.240	–	PtRh
46.75	1.941	1.95	PtRh
45.87	1.978	1.98	Pt_3O_4
68.25	1.373	1.37	PtRh

[a] Obtained from [24]

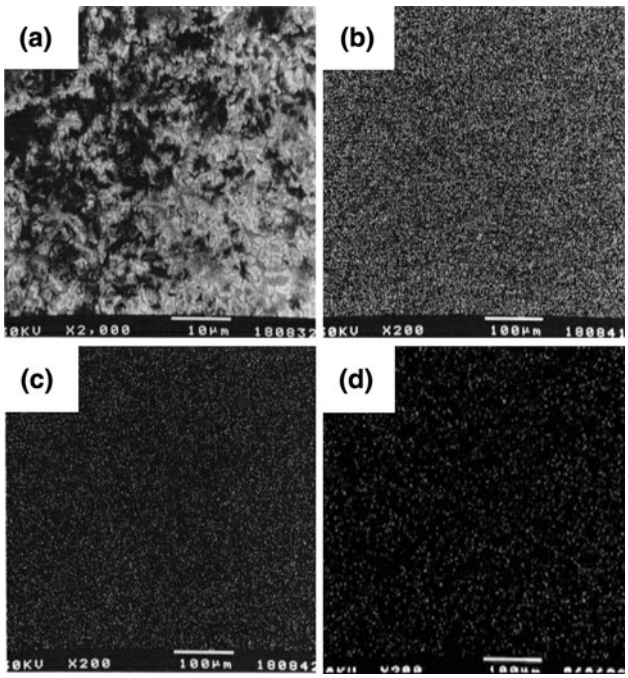

Fig. 4 SEM images and Hg mappings of quenched Pt–20% Rh surface after mercury electrodeposition and heating up to different temperatures: **a** SEM, 600 °C; **b** Pt mapping; **c** Rh mapping; **d** Hg mapping

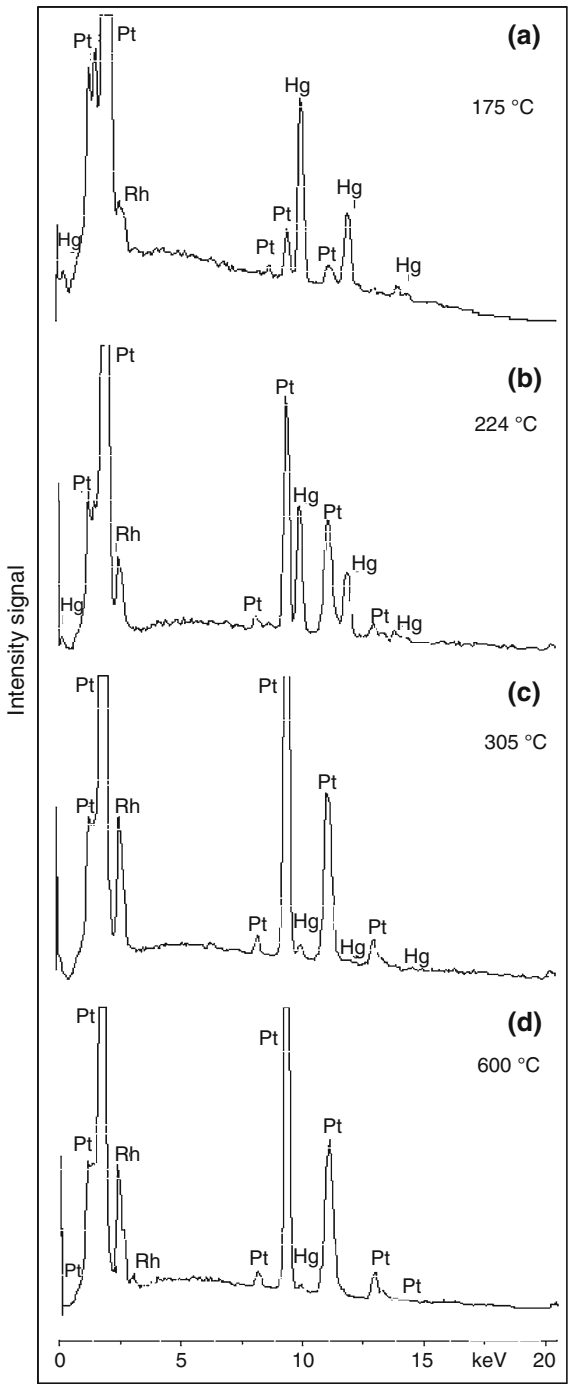

Fig. 5 EDX microanalysis of the surface quenched Pt–20% Rh alloy heating up to different temperatures at a sample time of 300 s: **a** 175 °C; **b** 224 °C; **c** 305 °C; **d** 600 °C. Electron beam acceleration: 30 kV

the end of the second step (T = 224 °C), showed, respectively, the presence of intermetallic compounds ($PtHg_2$, $RhHg_2$, and PtHg) and a homogeneous distribution of Hg atoms on the sample surface.

The third step of the TG curve (Fig. 1), which presents a slow kinetic, occurs from 224 to 305 °C (related to the third peak of the DTG), was attributed to thermal decomposition of a solid solution composed of the intermetallic species $RhHg_2$ and $PtHg_2$. For temperatures ranging from 224 to 305 °C, the mass loss is 8.02% of the total mercury electrodeposited for the third step. The presence of this intermetallic was confirmed by XRD (Table 3) for the system under study and is in agreement with the systems Pt–10% Rh/Hg [18], Pt–15% Rh/Hg, according to the reaction:

$$\left[RhHg_{2(s)} + PtHg_{2(s)}\right]_{\text{solid solution}} \rightarrow Pt + Rh + 4Hg_{(v)}.$$

For the sample subjected to heating to the final temperature of the third step of the TG curve (305 °C), the SEM image (not shown) shows a rough surface, containing PtHg and Pt, Rh, and Hg oxides, as determined by XRD (Table 3), not allowing the visualization of the grain boundaries. The results of mapping of Pt, Rh, and Hg, in agreement with the results of microanalysis by EDX (Fig. 5), revealed a significant decrease in the amount of Hg in the sample with the heating.

For temperatures above 305 °C, there is the presence of a continuous weight loss ramp, as sharp as observed earlier, for Pt_{pure}/Hg [23], Pt–10% Rh/Hg [18], and Pt–20% Ir/Hg [11] systems. However, samples of the Pt–20% Rh/Hg system, heated to a temperature of 600 °C, reveals the presence of Hg in the substrate, as revealed from the results obtained by techniques of microanalysis by EDX (Fig. 5) and Pt, Rh, and Hg mapping of chemical elements (Fig. 4b–d). Figure 4a shows the SEM image and the results of mapping of elements in the sample heated to 600 °C. The figure also shows a rough surface, not allowing the observation of the grain boundaries. The mapping for the element Hg (Fig. 4d) showed in the substrate of the mercury presence, in agreement with results of EDX (Fig. 5), suggesting that Hg diffuses to the sublayer.

Conclusions

The studies presented here allowed characterizing the mercury film formed on Pt–20% Rh alloy surface and also suggested intermetallic compound formation on the alloy surface. The film is formed by mercury electrodeposition on metal alloy foils followed by a reaction of mercury with the alloy surface probably assisted by heating at different temperatures.

The system Pt–Rh/Hg loses mercury in at least separate three steps: from the room temperature to 175 °C, only the bulk removed, and a solid solution of intermetallic compound film was found; between 175 and 224 °C, the second mass loss was attributed to the thermal decomposition of the intermetallic $PtHg_4$, generating $RhHg_2$ and $PtHg_2$; the third, from 224 to 305 °C, was ascribed to the decomposition of the $PtHg_2$ simultaneously with the $RhHg_2$ species.

EDX microanalysis has proved the presence of mercury on the grain surface and grain boundary after heating up to different temperatures, in agreement with the findings from the TG and DTG curves. The SEM images demonstrate that the grain boundaries and grain surfaces were attacked have a lower contact angle (Hg/subtract) and completely wet the foil surface. The SEM images obtained at 600 °C for Pt–20% Rh foil reveal a considerably roughening, which was also observed for pure Rh [16], Pt–10% Rh and Pt–30% Ir alloy [21] foils [18], which was also observed for pure Pt [17, 23], Pt–20% Ir alloy [11].

Acknowledgements Financial support to this work by the *Coordenação de Aperfeiçoamento de Pessoal de Nível Superior* (CAPES).

References

1. Joyner RW, Shpiro ES. Alloying in platinum-based catalysts for gasoline. Catal Lett. 1991;9:239–45.
2. Kizling MB, Stenius P, Anderson S, Frestad A. Characterization and catalytic activity of silicon-carbide powder as catalyst support in exhaust catalysts. Appl Catal B. 1992;1:149–68.
3. Xue E, Seshan K, Vanommen JG, Ross JRH. Studies on model reactions over a EuroPt-1 (Pt/SiO_2) catalysts. Appl Catal B. 1993;2:183–97.
4. Poirier GE, Hance BK, White JM. Scanning tunneling microscopy and Auger-electron spectroscopy characterization of a model catalyst-rhodium on TiO2 9001. J Phys Chem. 1993;97:5965–72.
5. Fierro JLG, Palacios JM, Thomas F. Characterization of catalyst and catchment gauzes used in medium-pressure and low pressure ammonia oxidation plants. J Mater Sci. 1992;27:685–91.
6. Awada M, Strojek J, Swain GM. Electrodeposition of metal adlayers on boron-doped diamond thin-film electrodes. J Electrochem Soc. 1995;142:L42–5.
7. Fleishmann M, Ponds S, Rolison D, Schmidt PP. Ultramicroelectrodes. Morganton: Datatech Science; 1987.
8. Whigtmann RM, Wipf DO. Voltammetry at ultramicroelectrodes. In: Bard AJ, editor. Electroanalytical chemistry. New York: Marcel Dekker; 1989.
9. Kreider KG, Tarlov MJ, Cline JP. Sputtered thin-film pH electrodes of platinum, palladium, ruthenium, and iridium oxides. Sens Actuator B. 1995;28:167–72.
10. Cumpson PJ, Seah MP. Stability of reference masses. I: Evidence for possible variations in the mass of reference kilograms arising from mercury contamination. Metrologia. 1994;31:21–6.
11. Fertonani FL, Benedetti AV, Ionashiro M. Contribution to the study of the reaction of mercury with platinum and platinum-rhodium alloy. Thermochim Acta. 1995;265:151–61.
12. Guminski C. The Hg-Pt (mercury-platinum) system. Bull Alloy Phase Diagr. 1990;11:26–32.
13. Massalski TB, Okamoto H, Subramanian PR, Kacprzak L. Binary alloy phase diagrams. 3rd ed. Materials Park: ASM International Press; 1990.
14. Kounaves SP, Buffle J. An iridium based mercury-film electrode. Part I: selection of substrate and preparation. J Electroanal Chem. 1987;216:53–69.
15. Affrossman S, Erskine WG. Thermal desorption of mercury from platinum surfaces. Trans Faraday Soc. 1966;62:2922–7.
16. Milaré E, Fertonani FL, Ionashiro M, Benedetti AV. Contribution to the study of the solid state reaction of mercury with puru rhodium. J Therm Anal Calorim. 2000;59:617–24.
17. Fertonani FL, Benedetti AV, Servant J, Portillo J, Sanz F. Electrodeposited thin mercury films Pt-Ir alloy electrodes. Thin Solid Films. 1999;341:147–54.
18. Ionashiro EY, Fertonani FL. Thermogravimetry (TG) applied to the study of the reaction of mercury with platinum-rhodium alloy. Thermochim Acta. 2002;383:153–60.
19. Milaré E, Ionashiro EY, Maniette Y, Benedetti AV, Fertonani FL. Influence of oxide deposition by repetitive cyclic voltammetry and controlled potential in reactivity of Ir with Hg. Port Electrochim Acta. 2003;21:69–78.
20. Milaré E, Ionashiro EY, Benedetti AV, Fertonani FL. Contribution to the study of Ir in aqueous solution of KNO_3/HNO_3 and $KNO_3/HNO_3/Hg_2(NO_3)_2$. Port Electrochim Acta. 2003;21:155–69.
21. Milaré E, Turquetti JR, Souza GR, Benedetti AV, Fertonani FL. Electrochemical study of the solid-state reactions of mercury with Pt-30%Ir alloy. J Therm Anal Calorim. 2006;86:403–10.
22. Fertonani FL, Milaré E, Benedetti AV, Ionashiro M. Contribution to the study solid-state reactions of mercury with pure noble metals. Part 2: mercury-iridium system. J Therm Anal Calorim. 2002;67:403–9.
23. Souza GR, Pastre IA, Benedetti AV, Ribeiro CA, Fertonani FL. Solid state reactions in the platinum-mercury system. Thermogravimetry and differential scanning calorimetry. J Therm Anal Calorim. 2007;88:127–32.
24. Affrossman S, Erskine WG, Paton J. Investigation of the poisoning of platinum group catalytic by thermal desorption. I. Mercury poisoning of benzene hydrogenation on platinum. Trans Faraday Soc. 1968;64:2856–63.